

Engineering of Neutral Excitons and Exciton Complexes in Transition Metal Dichalcogenide Monolayers through External Dielectric Screening

Sven Borghardt¹, Jhih-Sian Tu¹, Florian Winkler^{2,3}, Jürgen Schubert¹, Willi Zander¹, Kristján Lesson⁴, Beata E. Kardynał¹

1 Peter Grünberg Institute 9 (PGI-9), Forschungszentrum Jülich, DE-52425 Jülich, Germany

2 Ernst Ruska-Centre for Microscopy and Spectroscopy with Electrons (ER-C), Forschungszentrum Jülich, DE-52425 Jülich, Germany

3 Peter Grünberg Institute 5 (PGI-5), Forschungszentrum Jülich, DE-52425 Jülich, Germany

4 Innovation Center Iceland, Keldnaholti, IS-112 Reykjavik, Iceland

E-mail: b.kardynal@fz-juelich.de

May 2017

Abstract. In order to fully exploit the potential of transition metal dichalcogenide monolayers (TMD-MLs), the well-controlled creation of atomically sharp lateral heterojunctions within these materials is highly desirable. A promising approach to create such heterojunctions is the local modulation of the electronic structure of an intrinsic TMD-ML via dielectric screening induced by its surrounding materials. For the realization of this non-invasive approach, an in-depth understanding of such dielectric effects is required. We report on the modulations of excitonic transitions in TMD-MLs through the effect of dielectric environments including low-k and high-k dielectric materials. We present absolute tuning ranges as large as 37 meV for the optical band gaps of WSe₂ and MoSe₂ MLs and relative tuning ranges on the order of 30% for the binding energies of neutral excitons in WSe₂ MLs. The findings suggest the possibility to reduce the electronic band gap of WSe₂ MLs by 120 meV, paving the way towards dielectrically defined lateral heterojunctions.

Keywords: Transition Metal Dichalcogenides, Tungsten Diselenide, Molybdenum Diselenide, Exciton, Trion, Photoluminescence, Reflectance, Dielectric Screening, Lateral Heterojunction, Two-Dimensional Material

1. Introduction

Since the discovery of graphene the class of atomically thin two-dimensional materials has been growing continuously [1–4]. An exciting expansion of this class was done when transition metal dichalcogenide monolayers (TMD-MLs) were added to this material class [5]. In contrast to the semimetal graphene, TMD-MLs with the stoichiometric formula MX_2 , where M and X denote a transition metal atom (Mo, W, ...) and a chalcogen atom (S, Se, ...), respectively, are semiconductors with direct band gaps at the K -points of the hexagonal Brillouin zone with energies in the range of visible light [6]. Additionally, the heavy metal ions, the reduced Coulomb screening in two dimensions and the lack of inversion symmetry in these materials result in a unique combination of giant exciton binding energies, large spin-orbit coupling, as well as a coupling between the spin and valley degrees of freedom at the two inequivalent K -valleys that can be accessed optically [7–9].

Although there have been numerous reports on electronic and optoelectronic nanodevices made from TMD-MLs such as single-layer transistors, light-emitting diodes and photodetectors [10–12], there is a strong need to develop methods to create junctions. In analogy to well established semiconductor technology, where heterojunctions are the building blocks of most electronic and optoelectronic devices (e.g. laser diodes, HEMT transistors), the reliable creation of lateral heterojunctions within TMD-MLs would enable further development of next generation optoelectronic devices.

In analogy to three dimensional semiconductors where heterostructures are formed by interfacing materials of different chemical composition, lateral heterostructures of TMDs have been developed by introducing laterally

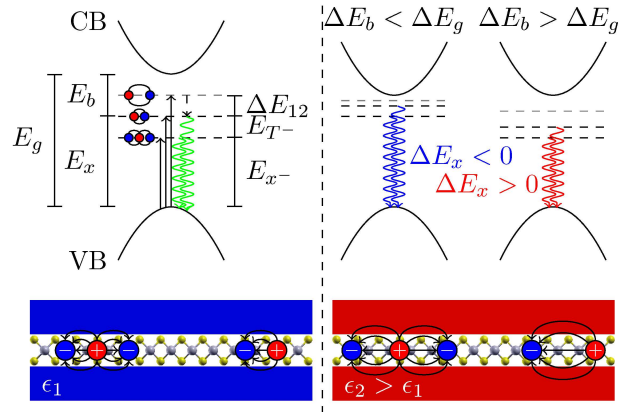


Figure 1. Schematic diagram of externally induced dielectric screening effects on the electronic and optical band gaps at the K -point of TMD-MLs. Solid arrows, dashed arrows and waved arrows represent optical absorption processes, non-radiative relaxation processes and radiative recombination processes, respectively.

varying stoichiometry [13, 14]. An alternative approach, which is unique to low dimensional materials, relies on the local modulation of screening of the ionic Coulomb potentials, as well as the Coulomb interaction between charge carriers, within the ML [15, 16] through a local variation of the relative permittivity of the ML’s direct environment, i.e. its substrate and cover material.

Fig. 1 depicts how externally induced screening changes both the electronic and optical band gaps of a TMD-ML. Both the electronic band gap, E_g , and the binding energy of the neutral exciton, E_b , in the monolayer are expected to decrease with an increasing relative permittivity of the surrounding dielectric [15–18]. The sign of the change of the optical band gap, $E_x = E_g - E_b$, depends on the relative change of these two quantities and can be probed optically by measuring the energy of free, neutral excitons. In addition to neutral excitons, charged exciton states (trions) with binding energies, $E_{T\pm} = E_x - E_{x\pm}$, on the order

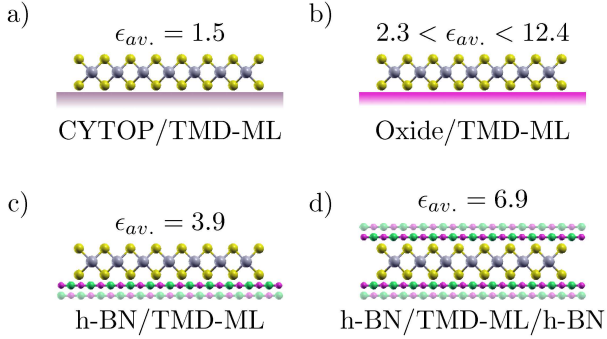


Figure 2. Symbolic diagram of the structures studied in this work, together with the average relative permittivity of the substrate and cover material in each structure.

of 30 meV have been observed in TMD-MLs [19–22]. Similarly to the binding energies of neutral excitons, the binding energies of trions in ML’s are expected to decrease with an increasing background relative permittivity [18]. Negatively charged trions are expected to be present in unbiased TMD-MLs, which are known to be unintentionally n-doped [19–22].

A first experimental evidence for the tunability of excitonic properties in TMD-MLs through environment-induced dielectric screening has been the report of a room temperature blue shift of E_x and E_{x^-} in MoS₂ MLs with an increasing relative permittivity of the non-ionic liquid with which the samples were covered [23]. More recently, an increase of the exciton Bohr radius in WSe₂ MLs with an increasing background relative permittivity of the surrounding material of the ML has been observed [24]. In addition, a decrease of the exciton binding energy and the electronic band gap has been observed for WS₂ MLs stacked with graphene [25].

In this work, we investigate different types of dielectrics as potential components of lateral heterostructure. We employ low temperature μ -photoluminescence, as well as reflectance measurements to study MoSe₂

and WSe₂ MLs. Our results show a red-shift of the optical band gaps, as well as a reduction of the binding energies of both the neutral exciton and the trion, with an increasing average relative permittivity of the ML’s surrounding. Estimates on the resulting changes of the electronic band gaps are made from the measured optical band gaps and exciton binding energies.

2. Experiments

Mechanically exfoliated WSe₂ and MoSe₂ MLs have been prepared on different substrates. The substrates were required to be flat in order to minimize the strain and the number of defects introduced in the TMD-MLs. Only transparent wide band gap materials were used. The substrates considered in this work can be separated into three types (fig. 2 a)-c)) according to their surface properties. The first type of substrate, namely CYTOP, is a low-k fluoropolymer, which is known for its chemical inertness and hydrophobicity. It is amorphous and transparent across a wide wavelength range and it features a very low relative permittivity for the entire frequency range. The second type are stable, transparent oxide substrates. Oxides offer a wide range of k-values but they are known to be hydrophilic. Hexagonal boron-nitride (h-BN) is a wide band gap layered material that can form van-der-Waals heterostructures with TMD-MLs. Similarly to CYTOP, h-BN is hydrophobic. A TMD-ML encapsulated by two hexagonal h-BN flakes was also included as a fourth dielectric environment (fig. 2 d)).

On a theoretical level, the effect of dielectric screening on excitonic properties is complex and non-analytic. Especially, an open question remains in which frequency domains the screening occurs. In our analysis, for the

sake of simplicity, we identify the surrounding materials by their static dielectric constant. This represents a simplification, however, we emphasize that it does not change the conclusions from this work. A more detailed discussion of this point can be found in the Supporting Information. The average nominal relative permittivity of the environment, $\epsilon_{av.} = \frac{1}{2}(\epsilon_{top} + \epsilon_{bottom})$, ranged from 1.5 for a TMD-ML on CYTOP to 12.4 for a TMD-ML on LaAlO_3 . All the layers in contact with the MLs were at least several nanometers thick and, as a consequence, only the layers in direct contact with the TMD-ML are needed to be included in the analysis.

μ -photoluminescence maps, as well as optical reflectance measurements of all structures were acquired at 11 K. While the former method only probes the emission energies of the ground states of neutral excitons and trions, absorption energies of the ground state, as well as of excited states, of the neutral exciton can be probed by the latter [26,27]. We further analyze the impact of charging induced by the substrate or the cover material as the reason for the observed effects.

3. Results

The emission energies of the neutral exciton and the trion of all structures shown in figure 2 have been measured in μ -photoluminescence experiments. Figure 3 shows photoluminescence spectra for three representative structures. The spectra contain signal from neutral exciton and trion recombination, as well as defect emission in the case of WSe_2 MLs. The energy of these peaks shows a systematic shift with $\epsilon_{av.}$. Figure 4, summarizes the emission energies for both the neutral exciton and the trion for all measured structures. The data points are averaged over large areas in

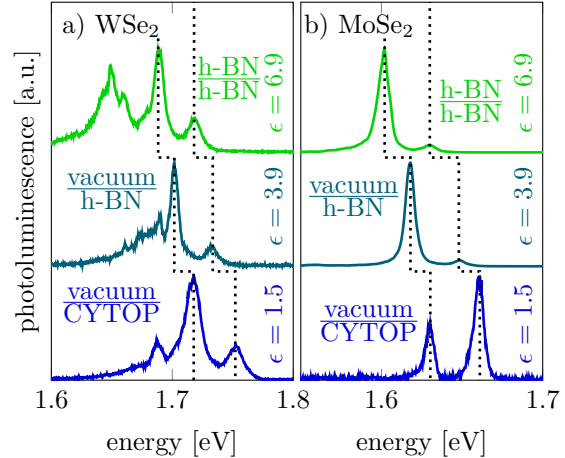


Figure 3. Representative photoluminescence spectra for WSe_2 (a) and MoSe_2 (b) MLs in different dielectric environments. The highest and second highest energy peak in each spectrum represent the neutral exciton and trion emission, respectively. For WSe_2 , a band of defects can be observed at the low energy end of the spectra. The dotted black lines connect the neutral exciton and trion emission peaks of each spectrum, as a guidance to the eye.

order to account for spatial variations of the peak positions. The trends in behaviour of WSe_2 and MoSe_2 MLs in different environments are very similar. The results for both TMD-MLs on SiO_2 , which is the most commonly used substrate, agree well with reports in the literature [19, 28]. There is a clear correlation in the positions of neutral exciton and trion peaks but there is no clear correlation with the nominal $\epsilon_{av.}$. Irrespective of the nominal relative permittivity of the substrate, the emission energies for MLs on CYTOP and for MLs on oxide substrates are very similar to each other and cluster around $(E_x, E_{x^-}) = (1.754\text{eV}, 1.717\text{eV})$ for WSe_2 and at $(E_x, E_{x^-}) = (1.664\text{eV}, 1.631\text{eV})$ for MoSe_2 . We attribute this effect to the presence of water on the hydrophilic oxide surface preventing a direct contact between the substrate material and the TMD-MLs. Hexagonal ice has a relative permittivity below 2 [29] and, thus, similar

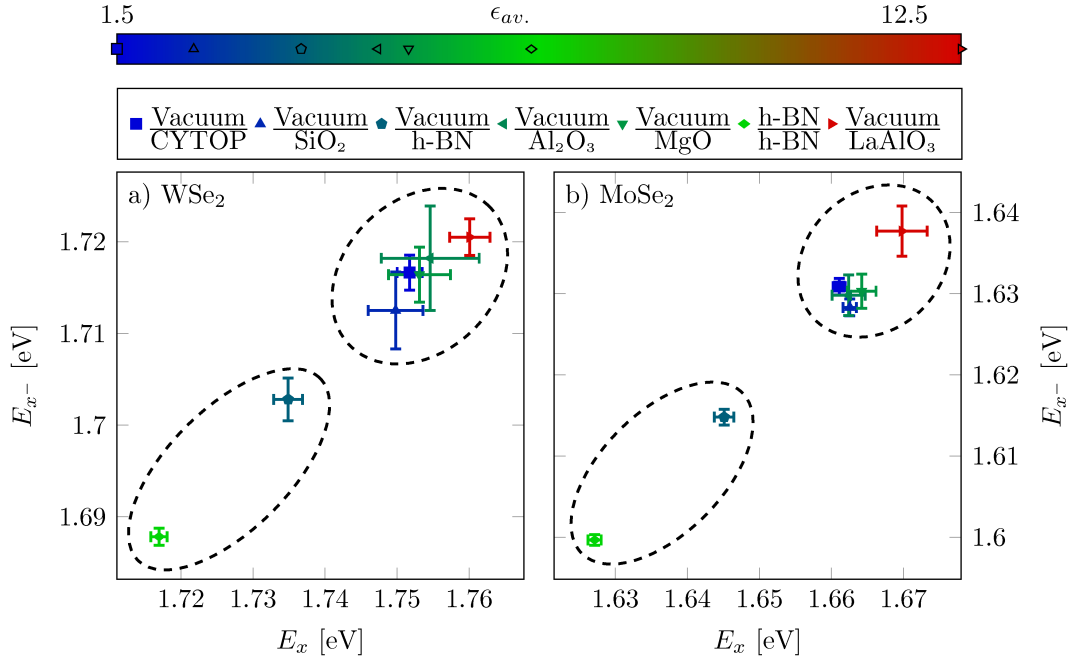


Figure 4. Emission energies of the neutral exciton and the trion in WSe₂ (a) and MoSe₂ (b) MLs for different dielectric environments. The legend shows the substrate and the cover material below and above the horizontal line, respectively. The color of the plotted data represents $\epsilon_{av.}$. The emission energies at each sample position have been obtained by hyperspectral fitting using a purpose-developed software (see Supporting Information) and the mean values and error bars are obtained by a pixel-by-pixel averaging over the sample area.

to that of CYTOP.

Even though the relative permittivity of h-BN is lower than that of some oxides, the emission energies of MLs on a h-BN substrate, as well as of MLs encapsulated in h-BN, show clearly observable red-shifts with respect to this cluster. For the neutral exciton, the red-shifts with respect to a ML on CYTOP are 17 meV (16 meV) and 35 meV (34 meV) for WSe₂ (MoSe₂) MLs on h-BN and encapsulated with h-BN, respectively. For the trion, the red-shifts with respect to a ML on CYTOP are 14 meV (16 meV) and 29 meV (31 meV) for WSe₂ (MoSe₂) MLs on h-BN and encapsulated with h-BN, respectively. It is well known that contamination is highly mobile in mechanically stacked van-der-Waals heterostructures clustering into so-called bubbles leaving behind large areas of

clean interfaces (Supporting Info, fig. 1) [30]. Since this contamination covers only a very small fraction of the sample area, the photoluminescence emission from the clean interfaces is expected to dominate the measured signal.

The observed red-shifts for the h-BN structures imply that the electronic band gap is undergoing a larger absolute change than the exciton binding energies when increasing $\epsilon_{av.}$. These findings are in contrast to previously reported observations in room temperature measurements of MoS₂ MLs in dielectric non-ionic liquids [23], but agree well with recent reflectance studies of TMD-MLs stacked with graphene [25].

Figure 5 shows the evolution of the trion binding energy, determined from the difference between neutral exciton and trion energies,

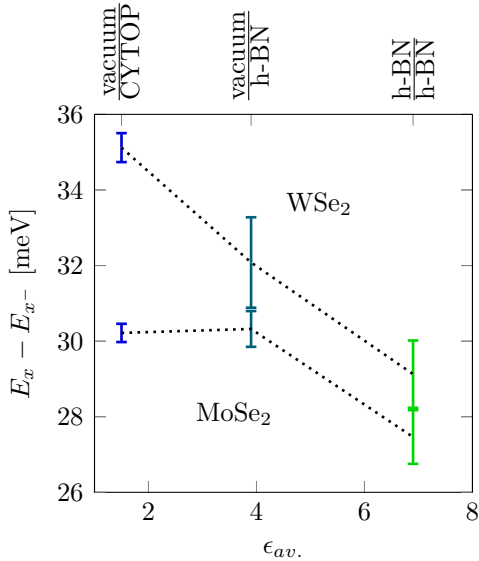


Figure 5. Trion binding energies in WSe₂ and MoSe₂ monolayers, as a function of ϵ_{av} . The binding energies at each sample position have been obtained by hyperspectral fitting using a purpose-developed software (see Supporting Information) and the mean values and error bars are obtained by a pixel-by-pixel averaging over the sample area.

as a function of ϵ_{av} , for MoSe₂ and WSe₂. For WSe₂ the trion binding energy decreases monotonically from 35 meV for a ML on CYTOP to 29 meV for a ML encapsulated in h-BN. This result is in good qualitative agreement with theoretical predictions [18]. In contrast, the trion binding energy of a MoSe₂ ML is nearly identical for a ML on CYTOP and a ML on h-BN. However, similarly to WSe₂, the trion binding energy of MoSe₂ decreases from 30 meV for a ML on h-BN to 27 meV for a ML encapsulated between two h-BN flakes. The small change between the trion binding energy of a MoSe₂ ML on CYTOP and a MoSe₂ ML on h-BN is still under investigation. A possible explanation may be a positive polarity of the trion for a ML on CYTOP, which, having a lower binding energy than negatively charged trions would cancel out the effect of the reduced screening

[28]. An indication for a different background charge for the ML on CYTOP is the different exciton-trion ratio observed in this structure (fig. 3). The trion binding energies are determined as the average difference between the exciton and trion emission energies and the standard deviations shown in figure 5 are up to five times lower than those determined for the exciton and trion emission energies themselves (fig. 4). This lower spatial fluctuation of the trion binding energy, indicates the robustness of excitonic binding energies against perturbations such as strain, as expected from theoretical studies [31]. Trion binding energies could thus be potentially used as a sensitive probe of surface state of transition metal dichalcogenide monolayers, providing a non-invasive alternative to the use of water droplets [32].

Changes of the optical band gap of TMD-MLs with spatially modulated ϵ_{av} are shown in figure 6 for a single MoSe₂ ML. The sample is prepared by placing the ML on an interface between SiO₂ and hBN and partially covering it with a hBN layer. While small variations of E_x within a region of constant ϵ_{av} are present, the correlation of E_x with the local ϵ_{av} of the TMD-ML is clear. The residual variations within each region are most likely due to strain variations, which are known to change the ML's electronic band gap [33]. A line profile across the boundary, that separates the part of the monolayer encapsulated in h-BN from the uncovered part on h-BN is shown in figure 6 c). In the line profile, it can be seen that the change of the optical band gap is observed over a distance of approximately 1.5 μm , which is the size of the laser spot in our measurements. Consequently, the band gap change is much more abrupt than the radius of the laser spot, which agrees well with theoretical predictions of the transition

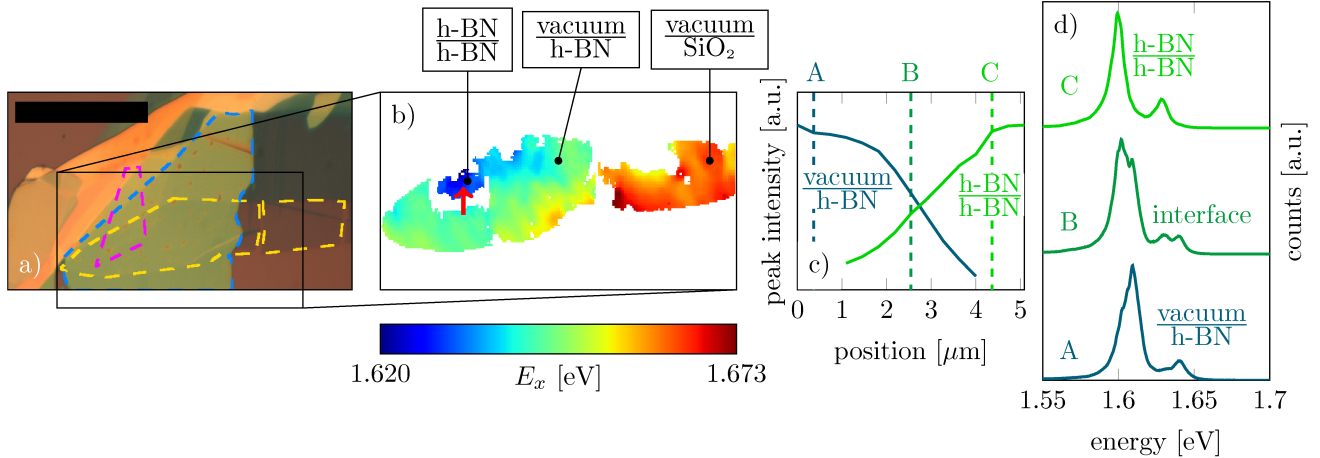


Figure 6. MoSe₂ monolayer in different dielectric environments. a) Optical micrograph of the TMD-ML (yellow line), which is partly lying on a SiO₂ substrate and partly lying on a h-BN flake (blue line). Furthermore, a part of the latter sample area is covered with another h-BN flake (magenta line). The scale bar is 20 μm . b) Spatial distribution of the exciton emission energy of the TMD-ML. Note that some pixels needed to be removed from the analysis when they showed disturbed photoluminescence spectra or when they probed two dielectric environments at the same time. c) Normalized intensities for the neutral exciton emission from the ML on h-BN and the ML encapsulated by h-BN along the a path marked by the red arrow in b). d) Representative spectra along the same path.

occurring across only a few crystal unit cells [15]. A representative spectrum from the interface between the two areas is shown in figure 6 d). It is a clear superposition of the peaks characteristics of each of the two areas. A line profile crossing the boundary between the ML area on h-BN and the ML area on SiO₂ cannot be analyzed, as there is no smooth transition of the photoluminescence signal observable. The height step between the two areas, which introduces strain or defects in the ML is most likely responsible for the distortions. The comparison between the two discussed interfaces demonstrates that the formation of well-defined, abrupt lateral heterostructures requires a change of the relative permittivity on a flat substrate.

Screening of Coulomb interactions at high carrier densities in TMD-MLs can lead to shifts in the exciton energies [34]. Such charges can be unintentionally introduced, for example, via substrate doping [35]. In order

to evaluate the possible role of doping we performed gate dependent photoluminescence experiments by contacting the device shown in fig. 6 with graphene as a contact. The results of the gate dependent photoluminescence experiments are shown in the Supporting Information (Supporting Information, Figure 2). It is apparent that, although the emission energies of both the neutral exciton and the trion are undergoing small changes if the gate voltage is changed, they are much smaller than the effect of the dielectric environment. In addition, different binding energies for negatively and positively charged trions can be seen, supporting the suggestion that the measured trion binding energy for a MoSe₂ ML on CYTOP can be explained by a positive polarity of the trion in this structure.

So far, the discussion has been limited to photoluminescence experiments, the results of which are of importance mainly for the design of new ultra-thin light sources with a tailored

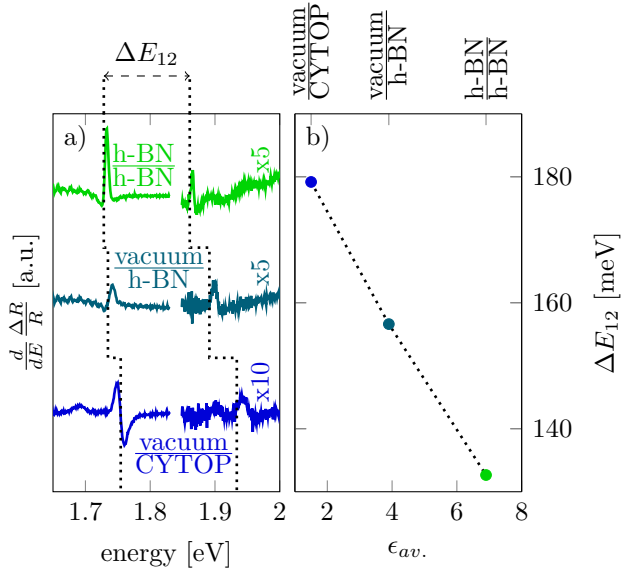


Figure 7. Reflectance contrast measurements for WSe₂ MLs in environments with different relative permittivity. a) shows the energy derivative of the reflectance contrast. The dotted lines connect the ground state and the first excited state of the neutral exciton of each spectrum, as a guidance to the eye. The positions of the ground state and excited state were determined by optimizing the energy derivative of the reflection contrast calculated using the transfer matrix method [36]. b) Energy splitting of the ground state and the first excited state of the neutral exciton, as a function of $\epsilon_{av.}$.

emission energy. However, the electronic band gap is also affected by the dielectric screening and understanding of the interplay between the two values may be of importance for trion confinement, as well as confinement in electronic devices. For this reason, we performed optical reflectance measurements which probe Rydberg series of the neutral exciton. The energy splittings in the Rydberg series are related to the exciton binding energy, the latter combined with optical band gap yielding an estimate of the electronic band gap [26]. The reflectance measurements were limited to WSe₂ MLs. The excited states of the neutral exciton overlap with the B-exciton in MoSe₂ MLs and, thus, cannot be measured

[37].

Due to the optical transparency of TMD-MLs, the effect of light reflection from the ML constitutes as small part of the total reflections from the sample. For this reason, reflectance contrast measurements need to be performed on such structures. The reflectance contrast is then given by $\frac{\Delta R}{R} = \frac{R_{ML} - R_{ref.}}{R_{ref.}}$, where R_{ML} and $R_{ref.}$ denote the reflectance from the ML region and the reflectance from a reference region without a ML structure, respectively. In order to make the features of the excited exciton states more pronounced, it is convenient to plot the energy derivative of the reflectance contrast, $\frac{d}{dE} \frac{\Delta R}{R}$ [26].

Figure 7 shows the energy derivative of the reflectance contrast of WSe₂ MLs for three measured samples together with the evolution of the energy splitting between the ground state and the first excited state of the neutral exciton, ΔE_{12} , as a function of $\epsilon_{av.}$. As in the photoluminescence experiments, the optical band gap is red-shifted. In addition, it is apparent that ΔE_{12} , and hence E_b , is decreasing with an increasing relative permittivity of the surrounding material of the ML. ΔE_{12} decreases monotonically from approximately 180 meV for a WSe₂ ML on CYTOP to almost 130 meV for a WSe₂ ML encapsulated by two h-BN flakes. Theoretical quasi two-dimensional calculations predict a relative change of 25% for the exciton binding energy when moving from a MoS₂ ML on h-BN to a MoS₂ ML encapsulated with h-BN, which agrees well with the measured relative change in ΔE_{12} of 16% [17].

For MoS₂ and WS₂ MLs on SiO₂, it has been shown that $E_b \approx 2\Delta E_{12}$, deviating from a classic hydrogenic model in three-dimensional semiconductors with $E_b = \frac{9}{8}\Delta E_{12}$ [26, 27]. With the assumption that this scaling factor is independent of the dielectric surrounding

of the TMD-ML, we estimate the absolute reduction in the exciton binding energy to be on the order of 90 meV when replacing the CYTOP substrate with h-BN encapsulation. A decrease of 120 meV, which is more than two times larger than the thermal energy at room temperature is obtained by combining the measured shift in the optical band gap with the reduction of the electron binding energy.

4. Conclusions

We have shown that h-BN is a suitable cladding material to tune the optical band gap of TMD-MLs whereas oxide substrates, irrespective of their relative permittivities, do not lead to a significant change in the optical band gaps of TMD-MLs.

A reduction of the optical band gaps of MoSe₂ and WSe₂ MLs by 37 meV was measured between the uncovered ML placed on a CYTOP substrate and a ML encapsulated in h-BN. In addition, a relative change of the exciton binding energy for WSe₂ MLs of approximately 30% was indirectly measured, which leads to an estimated reduction of the electronic band gap of WSe₂ MLs by 120 meV, when comparing uncovered MLs on a CYTOP substrate to a ML encapsulated in h-BN.

The energies of optical transition obtained in this work have been probed on the time scale of the exciton lifetime. It would be interesting to compare our results for the electronic band gap with scanning tunneling microscopy experiments, which probe the electronic band gap in the static limit.

We have shown that formation of optical lateral heterostructure purely by local variation of screening in three dimensions will require a control of the substrate flatness as well as substrate induced charge state. The latter is important to avoid energy transfer between

excitons and trions of different parts of the heterostructure.

In the heterojunction studied in this work (see fig. 6), the change from one region to another region was abrupt on the scale of the probe beam. Therefore, techniques with a better spatial resolution need to be developed in order to study dielectric effects on smaller length scales.

Our findings pave the way towards the creation of controlled lateral heterostructures, which are required as building blocks for next generation electronic and optoelectronic devices.

5. Acknowledgements

S. B. would like to thank Tony Heinz, Alexey Chernikov and Archana Raja for fruitful discussions and helpful advices.

6. References

- [1] Novoselov K S, Geim A K, Morozov S V, Jiang D, Zhang Y, Dubonos S V, Grigorieva I V and Firsov A A 2004 *Science* **306** 666–669
- [2] Li L, Yu Y, Ye G J, Ge Q, Ou X, Wu H, Feng D, Chen X H and Zhang Y 2014 *Nature Nanotechnology* **9** 372–377
- [3] Vogt P, Padova P D, Quaresima C, Avila J, Frantzeskakis E, Asensio M C, Resta A, Ealet B and Lay G L 2012 *Phys. Rev. Lett.* **108** 155501
- [4] Dávila M E, Xian L, Cahangirov S, Rubio A and Lay G L 2014 *New Journal of Physics* **16** 095002
- [5] Mak K F, Lee C, Hone J, Shan J and Heinz T F 2010 *Phys. Rev. Lett.* **105** 136805
- [6] Rasmussen F A and Thygesen K S 2015 *J. Phys. Chem. C* **119** (23) 13169–13183
- [7] Ugeda M M, Bradley A J, Shi S F, da Jornada F H, Zhang Y, Qiu D Y, Ruan W, Mo S K, Hussain Z, Shen Z X, Wang F, Louie S G and Crommie M F 2014 *Nature Materials* **13** 1091–1095
- [8] Cao T, Wang G, Han W, Ye H, Zhu C, Shi J, Niu Q, Tan P, Wang E, Liu B and Feng J 2012 *Nature Communications* **3**

- [9] Xiao D, Liu G B, Feng W, Xu X, and Yao W 2012 *Phys. Rev. Lett.* **108** 196802
- [10] Radisavljevic B, Radenovic A, Brivio J, Giacometti V and Kis A 2011 *Nature Nanotechnology* **6** 147–150
- [11] Ross J S, Klement P, Jones A M, Ghimire N J, Yan J, Mandrus D G, Taniguchi T, Watanabe K, Kitamura K, Yao W, Cobden D H and Xu X 2014 *Nature Nanotechnology* **9** 268–272
- [12] Lopez-Sanchez O, Lembke D, Kayci M, Radenovic A and Kis A 2013 *Nature Nanotechnology* **8** 497–501
- [13] Huang C, Wu S, Sanchez A M, Peters J J P, Beanland R, Ross J S, Rivera P, Yao W, Cobden D H and Xu X 2014 *Nature Materials* **13** 1096–1101
- [14] Mahjouri-Samani M, Lin M W, Wang K, Lupini A R, Lee J, Basile L, Boulesbaa A, Rouleau C M, Poretzky A A, Ivanov I N, Xiao K, Yoon M and Gehegan D B 2015 *Nature Communications* **6** 7749
- [15] Rösner M, Steinke C, Lorke M, Gies C, Jahnke F and Wehling T O 2016 *Nano Lett.* **16** 2322–2327
- [16] Ryou J, Kim Y S, KC S and Cho K 2016 *Scientific Reports* **6** 29184
- [17] Latini S, Olsen T and Thygesen K S 2015 *Phys. Rev. B* **92** 245123
- [18] Kylänpää I and Komsa H P 2015 *Phys. Rev. B* **92** 205418
- [19] Ross J S, Wu S, Yu H, Ghimire N J, Jones A M, Aivazian G, Yan J, Mandrus D G, Xiao D, Yao W and Xu X 2013 *Nature Communications* **4** 1474
- [20] Mak K F, He K, Shan J and Heinz T F 2012 *Nature Nanotechnology* **7** 494–498
- [21] Wang G, Bouet L, Lagarde D, Vidal M, Balocchi A, Amand T, Marie X and Urbaszek B 2014 *Phys. Rev. B* **90** 075413
- [22] Plechinger G, Nagler P, Kraus J, Paradiso N, Strunk C, Schller C and Korn T 2015 *physica status solidi (RRL)* **9** 457–461
- [23] Lin Y, Ling X, Yu L, Huang S, Hsu A L, Lee Y H, Kong J and Palacios M S D T 2014 *Nano Lett.* **14** 5569–5576
- [24] Stier A V, Wilson N P, Clark G, Xu X and Crooker S A 2016 *Nano Lett.* **16** 7054–7060
- [25] Raja A, Chaves A, Yu J, Arefe G, Hill H M, Rigosi A F, Berkelbach T C, Nagler P, Schller C, Korn T, Nuckolls C, Hone J, Brus L E, Heinz T F, Reichman D R and Chernikov A 2017 *Nature Communications* **8** 15251
- [26] Chernikov A, Berkelbach T C, Hill H M, Rigosi A, Li Y, Aslan O B, Reichman D R and Heinz M S H T F 2014 *Phys. Rev. Lett.* **113** 076802
- [27] Hill H M, Rigosi A F, Roquelet C, Chernikov A, Berkelbach T C, Reichman D R, Hybertsen M S, Brusand L E and Heinz T F 2015 *Nano Lett.* **15** 2992–2997
- [28] Jones A, Yu H, Ghimire N J, Wu S, Aivazian G, Ross J S, Zhao B, Yan J, Mandrus D G, Xiao D, Yao W and Xu X 2013 *Nature Nanotechnology* **8** 634–638
- [29] Kobayashi K 1982 *J. Phys. Chem.* **87** 4317–4321
- [30] Haigh S J, Gholinia A, Jalil R, Romani S, Britnell L, Elias D C, Novoselov K S, Ponomarenko L A, Geim A K and Gorbachev R 2012 *Nature Materials* **11** 764–767
- [31] Hui Pan H S, Zhang Y W and Yakobson B I 2013 *Phys. Rev. B* **87** 155304
- [32] Chow P K, Singh E, Viana B C, Gao J, Luo J, Li J, Lin Z, Elias A L, Shi Y, Wang Z, Terrones M and Koratkar N 2015 *ACS Nano* **9** 3023–3031
- [33] Johari P and Shenoy V B 2012 *ACS Nano* **6** 5449–5456
- [34] Steinhoff A, Rösner M, Jahnke F and Gies T O W 2014 *Nano Lett.* **14** 3743–3748
- [35] Sercombe D, Schwarz S, Pozo-Zamudio O D, Liu F, Robinson B J, Chekhovich E A, Tartakovskii I I, Kolosov O and Tartakovskii A I 2013 *Scientific Reports* **3** 3489
- [36] 2012 Multilayer thin film optics calculator <http://sjbyrnes.com/>
- [37] Wang G, Gerber I C, Bouet L, Lagarde D, Balocchi A, Vidal M, Amand T, Marie X and Urbaszek B 2015 *2D Materials* **2** 4

Engineering of Neutral Excitons and Exciton Complexes in Transition Metal Dichalcogenide Monolayers through External Dielectric Screening

Sven Borghardt,[†] Jhih-Sian Tu,[†] Florian Winkler,^{‡,§} Jürgen Schubert,[†] Willi
Zander,[†] Kristján Lesson,[¶] and Beata E. Kardynał^{*,†}

[†]*Peter Grünberg Institute 9 (PGI-9), Forschungszentrum Jülich, DE-52425 Jülich,
Germany*

[‡]*Ernst Ruska-Centre for Microscopy and Spectroscopy with Electrons (ER-C),
Forschungszentrum Jülich, DE-52425 Jülich, Germany*

[¶]*Innovation Center Iceland, Keldnaholti, IS-112 Reykjavik, Iceland*

[§]*Peter Grünberg Institute 5 (PGI-5), Forschungszentrum Jülich, DE-52425 Jülich,
Germany*

E-mail: b.kardynal@fz-juelich.de

Discussion of dielectric functions

In the following, details on the dielectric functions of the materials discussed in this work are given. The static relative permittivities of the materials in this work are shown in table 1. It can be seen that ice and CYTOP show the lowest relative permittivity. The oxide substrates offer a variety of relative permittivities some of which are lower and some of which are higher than the one of h-BN.

The frequency dependencies of the dielectric functions of the materials may be more involved. Exact results can be found in the literature.¹⁻⁵ Although the differences between the dielectric functions of all materials may vary as a function of the frequency, the main relations are conserved for frequencies up to approximately 20 THz. As a consequence, the requirements for the conclusions drawn in the main text, namely the low relative permittivities of ice and CYTOP, the diversity in the relative permittivities for the oxide substrates, as well as the low relative permittivity of h-BN compared with some of the oxide substrates, are fulfilled for a large range of frequencies.

Table 1: Static relative permittivities for the materials discussed in the main text. The values are taken from the literature.¹⁻⁵

Ice	CYTOP	SiO ₂	h-BN (\parallel)	h-BN (\perp)	Al ₂ O ₃ (\parallel)	Al ₂ O ₃ (\perp)	MgO	LaAlO ₃
1.9	2	3.5	5.06	6.85	9.7	11.3	9.3	23.7

Nano-bubbles in van-der-Waals heterostructures

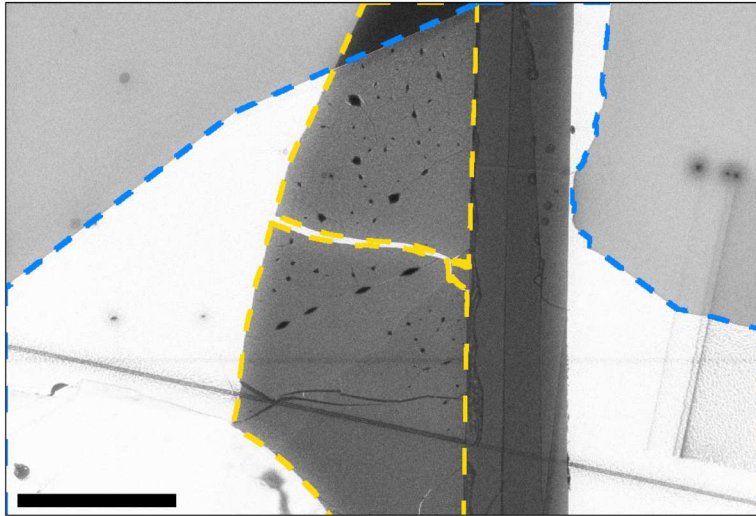


Figure 1: Scanning electron microscope image of a WSe₂ ML (yellow dashed line) placed on a h-BN flake (blue dashed line). Black spots can be observed at the van-der-Waals interface between the two materials. The black spots represent agglomerations of foreign material trapped at the van-der-Waals interface. It is apparent that the contamination only covers a small fraction of the entire sample area. The scale bar is 10 μ m.

Gate dependent photoluminescence experiment for different dielectric environments

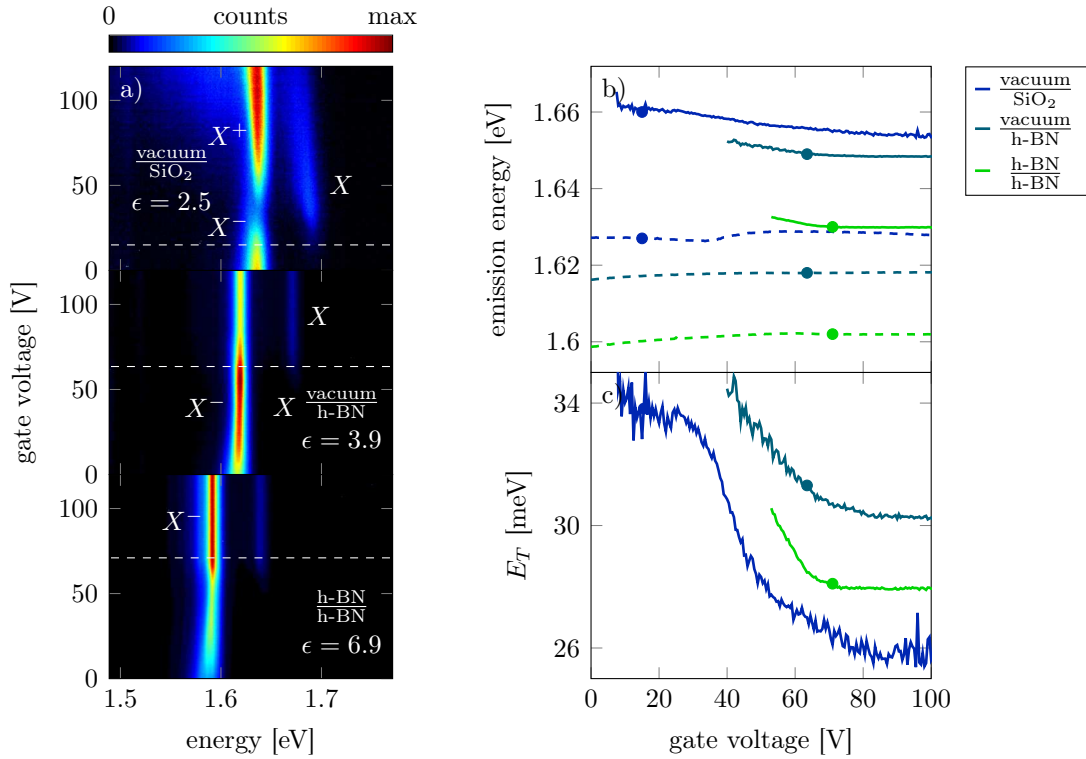


Figure 2: Gate dependent photoluminescence of a MoSe₂ ML in different dielectric environments. a) shows the photoluminescence signal as a function of the applied gate voltage. In all three dielectric environments, the negatively charged trion and the neutral exciton can be observed. On SiO₂, the positively charged trion can be observed as well. The white dashed lines mark gate voltages where the signal of the neutral exciton emission forms 5% of the total intensity. b) Emission energies of the neutral exciton (solid lines) and the trion (dashed lines) as a function of the applied gate voltage. c) Trion binding energy as a function of the applied gate voltage. The marks in b) and c) mark the gate voltages where the signal of the neutral exciton emission forms 5% of the total intensity.

Data analysis tool Py2DSpectroscopy

The hyperspectral data acquired in this work was analyzed using a home-developed analysis tool written in Python called Py2DSpectroscopy (figs. 3 and 4). The tool enables to browse hyperspectral data, align micrographs (e. g. AFM or SEM) with the data and fit the spectra included in the data. The source code is available on GitHub.⁶

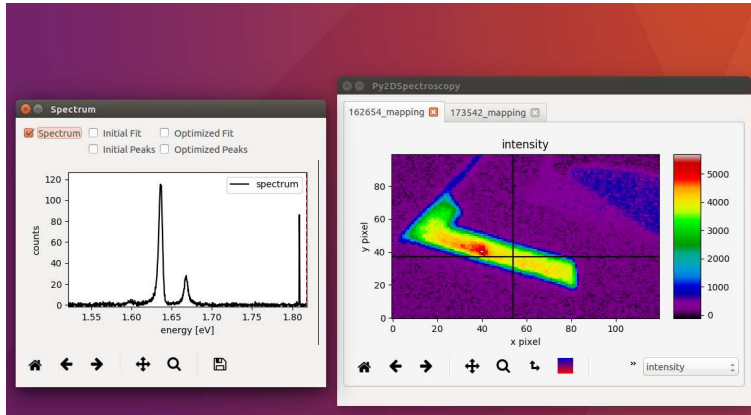


Figure 3: Browsing hyperspectral data using the Py2DSpectroscopy tool. The screenshot shows a colorplot of the integrated photoluminescence signal from a MoSe_2 monolayer on a LaAlO_3 substrate in the right window, as well as the spectrum at a specific position of the sample in the left window.

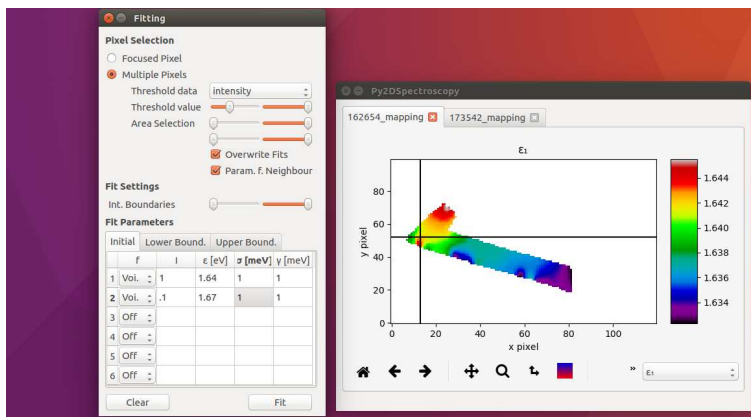


Figure 4: Fitting hyperspectral data using the Py2DSpectroscopy tool. The screenshot shows the fitting tool window on the left, as well as a colormap of the fitted emission energy of the trion from the same sample as in fig. 3 in the right window.

References

- (1) Kobayashi, K. Optical spectra and electronic structure of ice. *J. Phys. Chem.* **1983**, *87*, 4317–4321.
- (2) Bellex. <http://www.bellexinternational.com/products/cytop/>, Accessed: 2017-05-19.
- (3) Geick, R.; Perry, C. H.; Rupprecht, G. Normal Modes in Hexagonal Boron Nitride. *Phys. Rev.* **1966**, *146*, 543.
- (4) Aspnes, D. E.; Theeten, J. B. Dielectric function of Si-SiO₂ and Si-Si₃N₄ mixtures. *Journal of Applied Physics* **1979**, *50*, 4928.
- (5) Krupka, J.; Geyer, R.; Kuhn, M.; Hinken, J. Dielectric properties of single crystals of Al₂O₃, LaAlO₃, NdGaO₃, SrTiO₃, and MgO at cryogenic temperatures. *IEEE Transactions on Microwave Theory and Techniques* **1994**, *42*, 1886–1890.
- (6) SvenBo90/Py2DSpectroscopy: A simple Python UI script that can be used for the analysis of spectroscopy measurements on 2D materials, such as MoS₂. <https://github.com/SvenBo90/Py2DSpectroscopy>, Accessed: 2017-05-19.